PNAS PERSPECTIVE

Dating the Paleolithic: Trapped charge methods and amino acid geochronology

Kirsty E. H. Penkman[a,1], Geoff A. T. Duller[b], Helen M. Roberts[b], Debra Colarossi[b,c], Marc R. Dickinson[a], and Dustin White[a]

Edited by Suzanne Pilaar Birch, The University of Georgia, Athens, GA; received July 23, 2021; accepted August 12, 2022 by Editorial Board Member Dolores R. Piperno

Despite the vast array of different geochronological tools available, dating the Paleolithic remains one of the discipline's greatest challenges. This review focuses on two different dating approaches: trapped charge and amino acid geochronology. While differing in their fundamental principles, both exploit time-dependent changes in signals found within crystals to generate a chronology for the material dated and hence, the associated deposits. Within each method, there is a diverse range of signals that can be analyzed, each covering different time ranges, applicable to different materials and suitable for different paleoenvironmental and archaeological contexts. This multiplicity of signals can at first sight appear confusing, but it is a fundamental strength of the techniques, allowing internal checks for consistency and providing more information than simply a chronology. For each technique, we present an overview of the basis for the time-dependent signals and the types of material that can be analyzed, with examples of their archaeological application, as well as their future potential.

Quaternary | luminescence | electron spin resonance | racemization

1. Introduction

While radiocarbon dating has revolutionized the understanding of our archaeological past from the last ~60,000 y, earlier time periods are more opaque, restricted by the considerable challenges of dating beyond the limit of ^{14}C. The evolution and dispersal of hominin populations and the advances in tool technology and cultural development that occurred during the Paleolithic (the "Old Stone Age," covering hominin evolution and archaeology from ~3.3 million years [Ma] to ~20,000 years) took place during the major climatic oscillations that characterize the Quaternary (the most recent 2.6 My of Earth's history). These climatic changes resulted in periodic expansion of ice sheets into lowland areas; changes in sea level, temperature, moisture patterns, and aridity; and reorganization of plant and animal communities (1). Although a chronology of climate change over this period has been established from the relatively continuous marine and ice core records, most archaeological deposits are short and discontinuous, recording only snapshots of time, which have limited meaning in the absence of a broader chronological framework. This severely confines our understanding of how and when early humans may have evolved, migrated into, and adapted to new environments, and any influence on cognitive development and cultural identity.

One of the major archaeological challenges is, therefore, how to correlate sites with each other, both to piece together the often scattered archaeological record and also, to explore the links to records of climate and environmental change. A number of dating techniques (2) cover this longer time period (e.g., uranium series on speleothems and corals; tephrochronology, potassium-argon (K-Ar), and argon-argon (Ar-Ar) on volcanic deposits; paleomagnetism and biostratigraphy), but many of these rely on opportunistic sampling of suitable materials, which are rare, occur sporadically (e.g., tephra units, paleomagnetic reversals and excursions), or are restricted to specific environments (e.g., volcanic regions, karstic caves, coastal settings). This review, therefore, focuses on two approaches: trapped charge (luminescence and electron spin resonance [ESR]) and amino acid (AA) geochronology; they have different fundamental chemical/physical principles but share several commonalities. Both have the potential to cover the entire Quaternary time range and can be applied to materials that are commonly occurring and relatively stable over long timescales. The materials used for dating are also less restricted spatially, meaning these techniques can be used to link together sites both within and between regions. This review outlines the principles and capabilities of each technique, drawing together their potential to reveal insights into the early parts of our human story.

2. Trapped Charge Dating Methods

ESR and luminescence are trapped charge dating methods that use the ability of many naturally occurring crystalline materials to trap energy absorbed during exposure to ionizing radiation from the decay of potassium (K), uranium (U), and thorium (Th) and cosmic rays. This energy is stored by charge

Author affiliations: [a]Department of Chemistry, University of York, York YO10 5DD, United Kingdom; [b]Department of Geography and Earth Sciences, Aberystwyth University, Aberystwyth, Ceredigion SY23 3DB, United Kingdom; and [c]Department of Human Evolution, Max Planck Institute of Evolutionary Anthropology, 04103 Leipzig, Germany

Author contributions: K.E.H.P., G.A.T.D., and H.M.R. designed research; K.E.H.P., G.A.T.D., and H.M.R. performed research; and K.E.H.P., G.A.T.D., H.M.R., D.C., M.R.D., and D.W. wrote the paper.

The authors declare no competing interest.

This article is a PNAS Direct Submission. S.P.B. is a guest editor invited by the Editorial Board.

[1]To whom correspondence may be addressed. Email: kirsty.penkman@york.ac.uk.

Published October 17, 2022.

(normally electrons) in excited positions within defects in the crystal lattice and builds up over time. The trapped charge population is measured using ESR or luminescence and compared with the signal arising from exposure to a laboratory radiation source. This laboratory dose is called the equivalent dose (D_e) and is measured in the Système International (SI) unit of absorbed dose (gray). The age is calculated (Eq. **1**, units in parentheses) by dividing the D_e by the dose rate (gray per kiloannum [ka]), where the dose rate is the ionizing radiation dose received per unit time by the sample. This is determined by chemical analysis of the sample and the material around it to determine U, Th, and K concentrations or by direct measurements of the alpha, beta, and gamma radiation at the location where the sample was collected:

$$\text{Age (ka)} = \frac{\text{Equivalent dose (Gy)}}{\text{Dose rate } \left(\frac{\text{Gy}}{\text{ka}}\right)}. \quad \textbf{[1]}$$

A variety of different defects can occur in minerals caused by vacancies in the lattice or by the presence of impurities (e.g., Al or Ti substituting for Si in quartz). Different ESR and luminescence signals arise from these different defects. For ESR, the concentration of trapped charge in a defect is directly measured through microwave energy absorption as the strength of an applied magnetic field varies; the intensity of absorption at a particular resonance is proportional to the concentration of charge. In contrast, luminescence measurements involve exciting the trapped charge by stimulating the sample either with heat (producing thermoluminescence [TL]) or with light (generating an optically stimulated luminescence [OSL] signal).

The variety of ESR and luminescence signals and the different materials that can be analyzed can appear bewildering but are actually a major strength of the methods, providing a diverse range of approaches within these umbrella terms. Common to all trapped charge techniques are four key requirements that must be met for dating.

1) At some event of archaeological significance, the trapped charge within the crystal was set to zero or some defined level. This may be formation of the crystal (e.g., teeth used for ESR measurements), exposure to daylight in the case of OSL dating or ESR dating of sediments (a process known as optical bleaching), or being heated to high temperatures in a fire in the case of TL of burnt lithics.
2) The ionizing radiation dose rate has remained constant through time or can be modeled.
3) The trapped charge in the crystal is stable for a sufficiently long period of time compared with the event of interest for dating. As a rule of thumb, the lifetime needs to be at least 5 times greater than the event being dated and ideally, 10 times greater (3).
4) The concentration of trapped charge increases with exposure to ionizing radiation over the dating time period. Such an increase will not continue ad infinitum since there is a finite number of traps, and hence, above a certain value of absorbed dose, the trapped charge will not increase any further. This is called saturation, and trapped charge methods are limited by saturation of their signal.

ESR is commonly applied to fossil biominerals, while luminescence is typically applied to sediments containing quartz or feldspars. Such materials are ubiquitous, and it is rare for there not to be material suitable for luminescence dating at an archaeological site. Additionally, luminescence dating can be applied to fired materials and burnt lithics found at archaeological sites. Previous reviews have been written on ESR (4) and its recent applications (5) and on the use and history of luminescence in archaeology (6–8). This brief review outlines some of the most significant ESR and luminescence methods that are contributing to dating the Paleolithic and highlights some of the areas where recent advances are opening up new possibilities.

2.1. ESR. The use of ESR for geochronology was first described by Ikeya (9) applied to stalactites, and since then, it has been applied to a number of other materials, including corals, mollusks, tooth enamel, and quartz sediments (e.g., ref. 10). This current review will focus on just the last two as these have had the greatest impact in Paleolithic archaeology.

2.1.1. ESR of tooth enamel. One of the major advantages of ESR dating of tooth enamel is that the fossil material is directly dated. Tooth enamel (mainly carbonated hydroxyapatite [$Ca_{10}(PO_4)_6(OH)_2$]) yields a clear ESR signal, which can be used to assess the radiation dose up to a level of several thousand grays, therefore normally comfortably spanning the last million years. However, teeth may absorb or lose uranium during burial, causing the dose rate to change through time. Models of uranium uptake in early applications of ESR on teeth considered contrasting scenarios whereby either the elevated U concentrations in the teeth were absorbed early during burial (early uptake) or continuously during burial (linear uptake; e.g., dating the Florisbad skull, South Africa) (11). An alternative approach (12) combines U-series measurements and ESR to understand the changing concentration of uranium and its daughter products and hence, model the changes in dose rate through time. This combined approach (uranium series and electron spin resonance [US-ESR]) may also benefit from using laser ablation inductively coupled plasma mass spectrometry (LA-ICPMS) in order to map the U-series isotopes across a tooth fragment (13), thus allowing U-series ages to be determined at different points across a sample and providing data to allow calculation of the dose rate for ESR. The US-ESR approach has been applied to a wide number of key archaeological sites, such as the Rising Star Cave in South Africa to determine the age of *Homo naledi* to be between 236 and 335 ka (14) and Atapuerca, where an estimated age ranging from 949 to 624 ka was obtained (15). An additional advantage of the combined LA-ICPMS and ESR analyses of enamel is that it may be applied in a minimally destructive manner [Grün (16) has more discussion] since both methods may be applied to detached enamel fragments that can be later reinserted back into the fossil (Fig. 1).

2.1.2. ESR of quartz from sediments. Sediments are not normally prone to uncertainties in dose rate like teeth, and it is possible to measure a number of ESR signals from quartz (17, 18). Defect centers associated with Ti (Ti-Li or Ti-H) and Al substitution for Si in the quartz lattice yield ESR signals that grow to doses of >6,000 and >10,000 Gy, respectively (19), giving the potential to date over 2 Ma. However, two challenges have faced such applications. The event dated by ESR of sediments is the last exposure to daylight, but both ESR signals are reset slowly. Even after

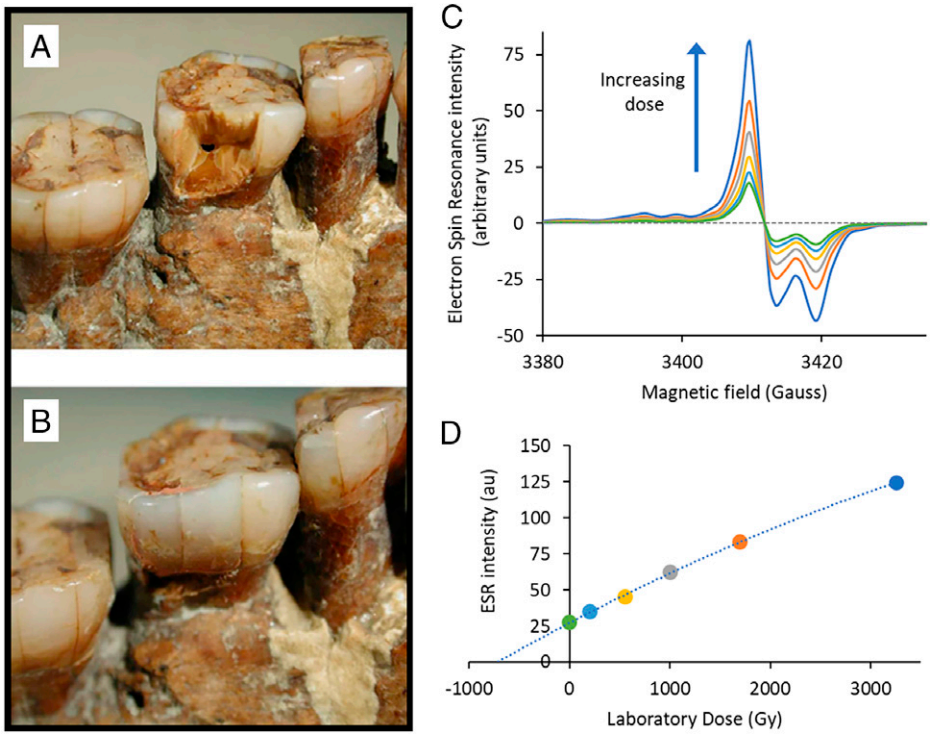

Fig. 1. (*A*) A tooth from the mandible of Tabun C1 after removal of an enamel fragment for combined U-series/ESR dating. (*B*) After analysis, the fragment was reinserted such that there is little visible impact upon the fossils. Photo by C. B. Stringer; reproduced with permission from ref. 16 (Elsevier). (*C*) Typical ESR spectra measured from tooth enamel. Different colors represent measurements after adding different laboratory radiation doses. (*D*) The increase in the intensity of the ESR signal in *C* with dose is used to characterize the dose–response of the sample and calculate the D_e (in this case, ~750 Gy). au, arbitrary unit. *C* and *D* were adapted from ref. 15.

34 d of exposure to a solar simulator (which is much more powerful than daylight), the Al signal retains ~50% of its signal (20), while the Ti-Li and Ti-H signals reach almost zero but only after exposure for 20 d (19). Thus, it is likely that neither ESR signal may be completely reset during deposition, and it is important to subtract this residual signal from the measured D_e. The second challenge is that while the Al signal has a lifetime of ~1.5 billion years [Ga], the Ti-Li and Ti-H signals appear to have a lifetime of only ~1.7 Ma at 10 °C (21) and are, therefore, prone to loss of signal and hence, age underestimation. In an analysis of ESR signals from quartz from a series of loess samples from the Luochuan site in the Chinese Loess Plateau covering the last 2.2 Ma, it was not possible to obtain ages beyond ~1 Ma, presumably because of loss of charge due to the low lifetime. Other studies have found different lifetimes for these signals (18), suggesting that it may be sample dependent. In summary, while the Ti-Li and Ti-H signals are reset by exposure to daylight more completely than the Al signal, the Ti signals are less stable, so care is needed in evaluating the results of this approach.

Nevertheless, many archaeological sites have been dated using these multiple quartz ESR signals, such as the earliest Acheulian sites across northwestern Europe (22), including the French site of Moulin Quignon at 670 to 650 ka (23). However, the complexity involved in applying ESR (with issues of incomplete resetting of the signal and signal instability) is illustrated by the work at Tourville-la-Rivière, France (24). Reproducible ages (~330 ka) were obtained for a silty–clayey sedimentary unit, while two sandy units showed ages ranging from ~250 ka to more than 1.2 Ma. The scatter in ages for the sandy units is thought to result from incomplete resetting of the Al center, but it seems that both the Ti-Li and Al centers for all three units were incompletely reset due to the nature of the fluvial deposition. In contrast, the Ti-H center ESR ages are in agreement with the US-ESR ages of fossil teeth, illustrating its potential for dating late Middle Pleistocene deposits (24). Unlike luminescence, where single-grain analysis can assess whether sediments have been heterogeneously bleached at deposition (*Section 2.2.1*), ESR measurements typically need 150 to 200 mg of purified quartz per measurement, and in total, 1 to 2 g may be needed; therefore, this approach is not possible. Instead, the multiple center ESR dating approach first proposed by Toyoda et al. (25) and deployed at Tourville-la-Rivière is the only way to assess the potential for incomplete bleaching (24), capitalizing on the different propensities for bleaching of the Al and Ti centers.

2.2. Luminescence Dating. Like ESR, luminescence methods utilize trapped charge that accumulates in minerals. Unlike ESR, the trapped charge is released during measurement, and the energy stored leads to the emission of light; this is luminescence. The trapped charge may be stimulated in the laboratory by heating the sample (typically to about 500 °C) giving TL or by light at a particular wavelength. The luminescence emitted at a different wavelength is measured and termed OSL (26). Blue or green light (~470 or 530 nm) is commonly used for stimulation of quartz, and the resulting OSL signal is observed in the near ultraviolet (UV, ~340 nm). In some studies, terms such as infrared-stimulated luminescence (IRSL), commonly applied to feldspars, or violet-stimulated luminescence are used, denoting the different wavelengths of the light used for stimulation.

Luminescence may date different types of events, commonly heating of the sample or exposure of the mineral grains to daylight. The two minerals most widely used for luminescence dating are quartz and feldspar, both very common detrital minerals on the Earth's surface.

2.2.1. Luminescence in quartz. A widely used signal from quartz is the OSL signal, which has a lifetime when stored at ∼20 °C estimated at 210 Ma (27). An additional advantage of this signal is that it is reset by exposure to daylight in a short period of time (typically less than a minute in sunlight). The main limitation is saturation of the OSL signal, which typically limits the application to the last ∼150 ka, although in areas where the dose rate (Eq. **1**) is low, older ages are possible.

Archaeological sites may be prone to disturbance, which can mix sediment grains from one unit to another; however, such disturbance is not always clearly visible. One approach to deal with such uncertainty is to measure OSL from single sand-sized grains of quartz [∼200 μm in diameter (28)], where D_e is calculated for many tens or hundreds of individual grains (e.g., Fig. 2*B*). Clarkson et al. (29) dated 52 samples from Madjedbebe in northern Australia (measuring 25,700 grains), demonstrating the continuity of accumulation at this site over the last ∼80 ka and providing an age of 65.0 ± 5.7 ka for the first site occupation, which makes it the earliest suggested evidence for humans in Australia. However, where a sample has cross-cut a boundary [e.g., as seen at Sibudu, South Africa (30)] or in units contaminated by materials of a distinctly different age (e.g., roof spall degrading within an occupation layer), this is seen in the pattern of D_e values, and statistical models need to be applied to derive an accurate value of D_e for age calculation (31).

Single-grain luminescence measurements make many determinations of D_e for a sample, but a common assumption is that the dose rate (the denominator in Eq. **1**) is the same for all grains within the sample. However, grains of potassium-rich feldspar are common (containing up to 14% potassium concentrations), and zircons or other heavy minerals with concentrations of U and Th of many tens or hundreds of parts per million may also be present. These high levels of radionuclides may produce radiation hot spots, where dose rate is many times the average value. Conversely, where carbonates are present, it is possible that dose rates may be lower than average. Assessing the magnitude of these small-scale variations (often termed microdosimetry) has proven challenging and been tackled variously by modeling (32), measurement of chemical composition (33), or measurement of spatial variations in beta dose (34).

The other challenge facing quartz OSL is saturation. The defects within quartz that store charge measured by OSL typically become full after receiving doses of ∼100 to 200 Gy, although this varies from one sample to another and even from one grain to another within the same sample (e.g., refs. 35 and 36). As samples approach saturation, the uncertainty in the calculated age becomes larger because of the low slope of the dose–response curve and the potential for systematic errors (37).

To circumvent saturation of the OSL signal in quartz, other signals that arise from different traps and that continue growing to much higher doses have been sought. One signal is the thermally transferred optically stimulated luminescence (TT-OSL) signal first described by Wang et al. (38), where it was shown that the signal continued to grow far beyond 4,000 Gy, at least an order of magnitude larger than typical OSL signals from quartz. While the OSL signal from quartz is related to a TL peak at 325 °C, the TT-OSL signal is thought to relate to a number of different TL peaks, including that at ∼375 °C. TT-OSL measurements on single grains have been used to date sites in northern Spain (39), including the Sima de los Huesos hominin fossils at Atapuerca dated to 448 ± 15 ka (40). Multiple grain TT-OSL measurements have been undertaken at Kalambo Falls, Zambia (41), where the mode 2/3 transition was dated to between ∼500 and 300 ka (Fig. 2), and also at the early Middle Stone Age site at Wonderwerk Cave in South Africa, yielding a sequence of ages from 238 ± 13 to 153 ± 15 ka (42). Although promising, the TT-OSL signal is only reset slowly by sunlight compared with the OSL signal, and some studies suggest that the signal has a lifetime of 4.5 Ma at 10 °C (43); this would imply that ages should be corrected for loss of signal during burial (41). However, the stability of the signal is still debated, with some suggesting even lower stability (44) and others finding that no correction for lifetime is required (45).

An alternative approach for increasing the age range over which quartz can be dated is to look at quartzite or

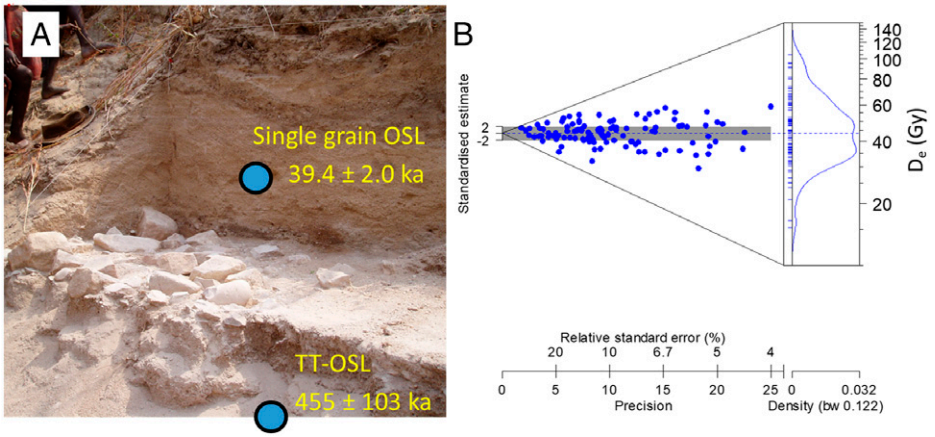

Fig. 2. (*A*) Close-up view of part of the excavation at Kalambo Falls, where both single-grain OSL and TT-OSL have been used. (*B*) Each dot is an OSL D_e value for one individual grain of quartz from the uppermost sample shown in *A*, and the probability density function on the right of the plot shows the distribution of measured D_e values. bw, bandwidth.

vein quartz cobbles (~20 to 100 mm in diameter). As the cobble is primarily quartz (SiO_2), the environmental dose rate is very low, thus extending the age range. Bailiff et al. (46) tested this approach on a number of sites in the United Kingdom and Portugal, and demonstrated that it was able to date back to 500 ka and possibly as far as 1 Ma.

2.2.2. Luminescence in feldspar. Feldspar occurs in a range of compositions (a solid solution series exists from $KAlSi_3O_8$ to $NaAlSi_3O_8$ to $CaAl_2Si_2O_8$). Studies have either focused on silt-sized grains (typically 4 to 11 μm in diameter), where feldspar mineral separation is not feasible, or potassium-rich feldspars for sand-sized grains (typically 180 to 212 μm in diameter), where differences in density can be used to separate minerals. Feldspar can be optically stimulated using infrared (IR, ~850 nm). In comparison with quartz OSL, this IRSL signal from feldspars grows to a higher radiation dose, thus potentially allowing older ages to be determined. For many years, luminescence dating with feldspar was overshadowed by signal instability termed "anomalous fading" (47), causing age underestimation. A variety of methods for measurement and correction of this loss of signal were determined (e.g., ref. 48). However, a major breakthrough was to realize that after making the initial IRSL measurement (while holding the sample at ~50 °C), a second measurement of the IRSL signal while holding the sample at a higher temperature (typically 225 °C or 290 °C) yielded a more stable signal (49), minimizing the impact of anomalous fading. This post-IR (pIR) IRSL signal has been applied widely since its first discovery, and as understanding of the underlying physical processes develops, the pIR IRSL method continues to evolve (e.g., ref. 50).

Roberts et al. (51) used pIR $IRSL_{225}$ to date an ~90-m-long core from Lake Tana in Ethiopia to provide a paleoenvironmental framework for understanding hominin evolution and dispersal in this climatically sensitive and fossil-rich region. Luminescence ages overlapped with those from radiocarbon in the upper ~25 m of the core, but below this, the pIR IRSL ages were the only means of dating this critical record, which extends back to ~250 ka. Feldspars also offer the opportunity to date older sediments than is possible with quartz, and Jacobs et al. (52) present data for 92 samples to constrain the age of the sediments in Denisova Cave in southern Siberia, the type locality of Denisovan hominins that also preserves evidence of Neanderthal and modern human occupation (53). The combination of quartz and potassium-rich feldspar single-grain measurements showed that hominin occupation of the site had occurred from 300 to 20 ka.

2.2.3. Luminescence in other materials. ESR dating of quartz and luminescence dating of sediments offer the advantage of working with materials that are typically ubiquitous, and hence, an age can be determined in a variety of depositional settings. However, for these materials, it is important to determine the association between what is being dated and the archaeological record that is of interest. TL dating of burnt cobbles and flint artifacts (54) provides much clearer archaeological association. Although not widely applied, these techniques have played a central role in elucidating the age of some key sites; perhaps the most notable recent example is Jebel Irhoud in Morocco, where analysis of burnt flint artifacts associated with the remains of *Homo sapiens* yielded an age of 315 ± 34 ka, currently the oldest example of our species (55).

Some of the earliest work using luminescence for geochronology was undertaken on limestones (56) and biogenic calcites (57). Their TL signal grows to high doses before saturating, but a major challenge measuring biogenic calcite has been removal of any original organic matrix. Organic material produces spurious TL signals when it is heated to the temperatures necessary to obtain the dosimetric signal. Additionally, the TL is emitted at ~580 nm, on the limit of the photomultipliers typically used for dating. However, recent research on calcitic slug plates (58) and snail opercula (58, 59) has shown that these biominerals have a negligible organic matrix, and by using recently developed electron-multiplying charge coupled device (EMCCD) cameras sensitive across a wide wavelength range, a TL signal can be measured (60). Using an EMCCD to image the TL signal (Fig. 3) also makes it possible to map the apparent age across the surface of the sample. This provides a check on whether the sample has been affected by diagenesis. The two main TL peaks have lifetimes of ~70 Ma and ~140 Ga (59), and both give signals that grow to doses of more than 8,000 Gy, implying that it should be feasible to date back to at least 4 Ma. The TL signal from *Bithynia tentaculata* opercula collected from Purfleet, part of the Thames terrace sequence, yielded an age of 316 ± 22 ka (61), consistent with both an OSL age from quartz of 329 ± 30 ka and an amino acid correlation of the site using *B. tentaculata* opercula with marine oxygen isotope stage 9 (MIS 9) (62). This new TL method has exciting potential to provide a chronological framework for Paleolithic sites where suitable biogenic calcites are found; fortunately the freshwater habitats needed for these molluscan species were also attractive to early hominins.

3. AA Geochronology

AA geochronology is based on the time-dependent breakdown of proteins in fossils. Proteins play an important role in biomineralization and are, therefore, incorporated into these skeletal hard parts. Some of these proteins (and their AA building blocks) are retained in fossil biominerals (such as shells, corals, and teeth), enabling them to be used for dating. The rates of these breakdown reactions mean that the technique can date the whole Quaternary period, from ~20 y ago to at least 3 Ma (63). In archaeological contexts, it is most useful for dating sites older than ~40 ka, providing valuable insights into relative age and numerical age if calibrated.

3.1. Principles of AA Dating. Every protein is composed of chains of AAs in specific orders (a "sequence") connected by peptide bonds. Each AA has an α-C, to which is bonded an amino group ($-NH_2$), a carboxylic acid (-COOH), a hydrogen (H), and a side chain (R); this R group designates the type of AA. Of the 20 proteinogenic AAs, all but glycine (which has H as its side chain) have a chiral center at the α-C. This chiral center means that these AAs can exist in two nonsuperimposable mirror images of each other (Fig. 4*A*), termed left handed (laevo, L form) and right handed (dextro, D form).

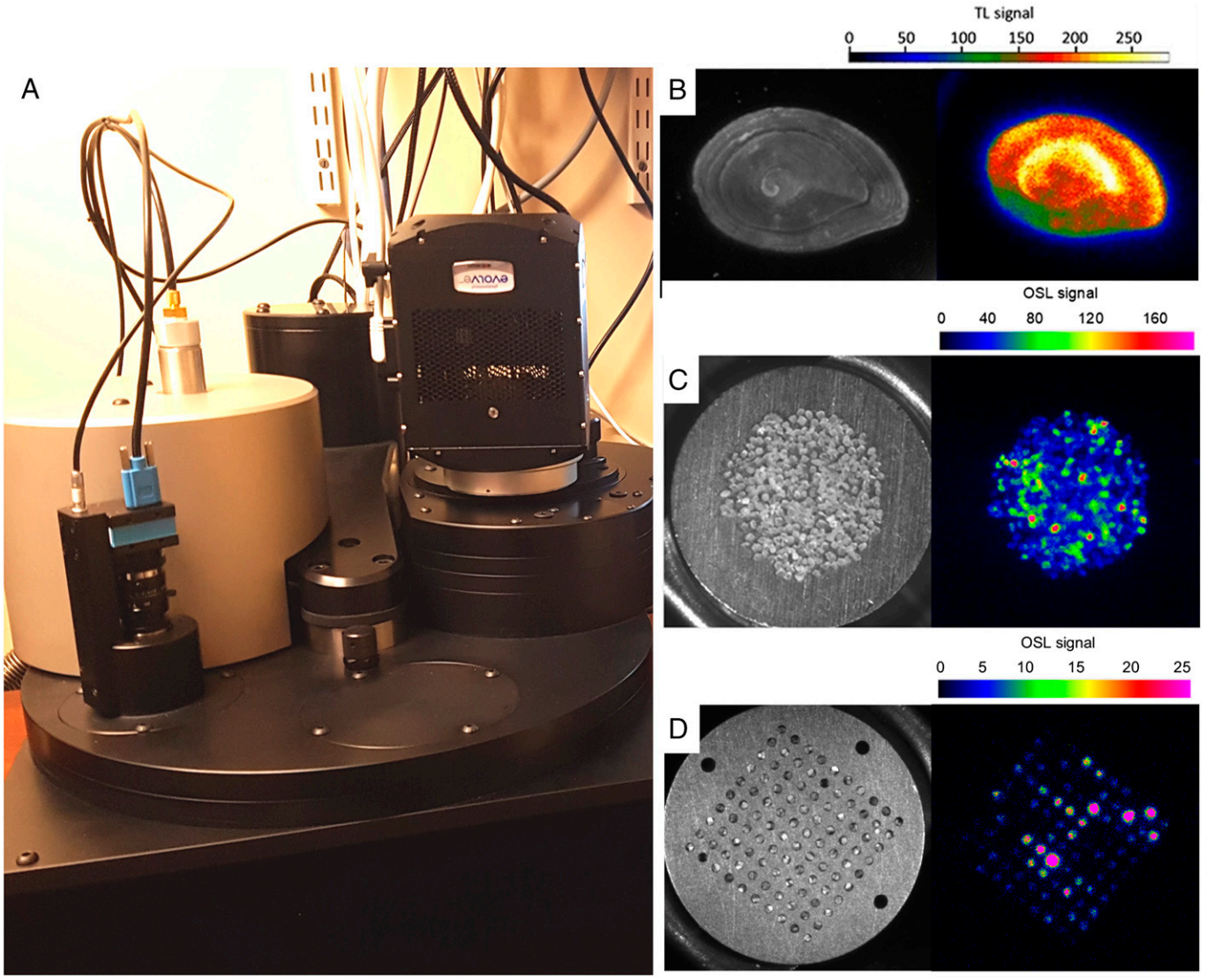

Fig. 3. (*A*) EMCCD for imaging luminescence signals. (*B*) An operculum from *B. tentaculata* (~4 mm on the longest axis) and its TL signal. As well as imaging TL from opercula, the EMCCD also permits imaging of OSL signals from quartz grains on a 9.8-mm-diameter sample holder (*C*) or quartz grains mounted in a single-grain disk (*D*).

In living organisms other than bacteria, proteins are exclusively synthesized from the L form. However, after death or on cessation of tissue turnover, a spontaneous reaction called racemization occurs, increasing the amount of the D form over time. The extent of racemization is recorded as a D/L value, which gradually increases from near zero in modern samples to an equilibrium (in most cases to approximately one, where the D and L forms are present in equal proportions). Depending on the AA, this can take tens of thousands to millions of years.

Using both fossil samples and experiments on modern material (e.g., refs. 64–67), the three main protein diagenetic changes are:

1) racemization (an increase in D/L value);
2) hydrolysis of the peptide bond, breaking up the protein chain (increase in free AAs); and
3) decomposition of the AAs (decrease in concentration).

These reactions are intimately linked (Fig. 4*B*). Hydrolysis breaks the peptide bond between two AAs within a protein chain, leaving them at the end of the chain (terminal AAs) and able to more freely racemize; further hydrolysis creates free AAs, which then decompose. At any moment, there will be AAs bound tightly in protein chains, AAs at terminal positions, and free AAs, all with different rates of racemization and breakdown. Additionally, some AAs, such as aspartic acid and serine (68), are able to racemize while in the protein chain. Each type of AA also racemizes at a different rate due to the chemical effects of the differing side chains.

Protein degradation, therefore, consists of a series of chemical reactions, which are interrelated, and these different reactions can provide multiple "clocks" within a single sample, with different time ranges and resolutions. However, as chemical reactions, in an open system of protein their rates will be dependent not only on time but also on environmental factors. Early studies, therefore, probed the effects of factors, such as temperature, pH, metal ions, and the availability of water on the rates of racemization. It was concluded that leaching of original protein caused significant problems in some biominerals, such as bone (69), but that others (such as mollusk shell) seemed to provide greater protection for the protein (70).

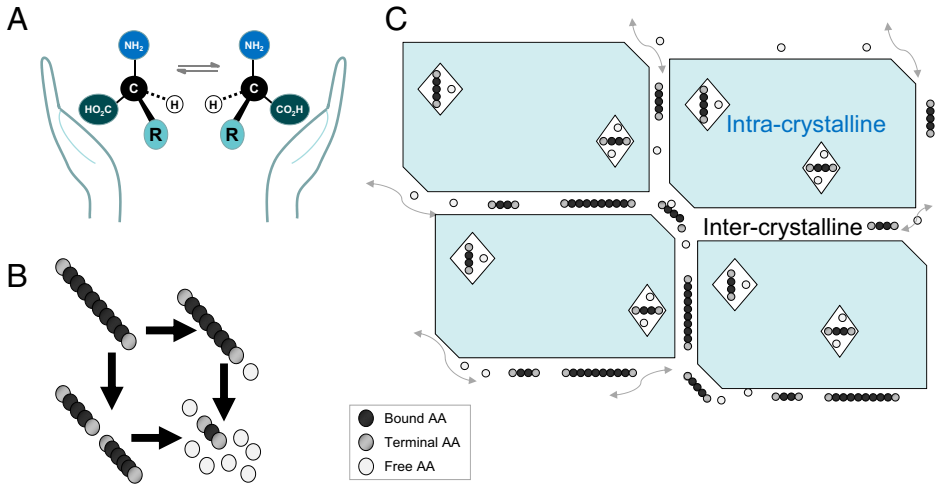

Fig. 4. (*A*) Most AAs have four different groups attached to the α-C, so their mirror images are nonsuperimposable (just like hands) and therefore, distinct from each other. (*B*) Peptide bond hydrolysis breaks up protein chains, creating shorter peptides, terminal AAs, and ultimately, free AAs. This occurs during natural diagenesis in the fossil but also, as part of the laboratory preparation process, with subsampling enabling analysis of the total hydrolysable AA fraction as well as the free AA fraction. (*C*) Schematic of the intercrystalline AAs (between the crystallites) and the intracrystalline AAs (hypothesized to be trapped within the faceted voids in some biominerals, as imaged in ref. 75). The intercrystalline protein is likely to be subject to diffusive loss over time as well as being impacted by the environment; effectively operating as a closed system, the IcP degradation should, however, be predictable and only dependent on time and temperature.

3.2. Toward a Closed System Approach. As the impact of environmental factors (e.g., pH, availability of water) could never be known for an individual sample, this led to analyzing "closed system" protein from fossil samples, focusing on analyzing a fraction of protein that is physically or chemically shielded from the environment and therefore, for which protein breakdown is solely time and temperature dependent. Hints at the presence of a closed system of protein within Paleozoic shells (71) led to the hypothesis that "organic material trapped within single crystals during biomineralisation offers the best hope for the study of ancient fossil proteins" (ref. 72, p. 73). This chemically protected organic matter is defined as the "intracrystalline" fraction (Fig. 4*C*), with evidence of closed system behavior in this fraction in eggshell (73, 74) and some biominerals treated with strong oxidants, such as bleach (75–79), although importantly, not for all biominerals (80–83). Isolation of this intracrystalline protein (usually abbreviated to "IcP") has provided useful age information in shells, eggshells, foraminifera, ostracods, and tooth enamel; in long-lived biominerals (e.g., corals), it can even provide age information within an individual (84).

3.3. Building an Aminostratigraphy. The age of a sample can be determined based on 1) which AA reactions are tracked, 2) the genus/species (of biomineral) being analyzed, and 3) a baseline reference framework (an aminostratigraphy) (e.g., refs. 85 and 86) of comparative data from sites that have experienced the same effective diagenetic temperature history. Assessment of protein/AA breakdown is achieved from a single chromatographic analysis of an individual sample, with age estimates for a horizon ideally based on the analysis of ≥ three individuals.

3.3.1. Taxonomic effect. Different taxa have different biomineral protein sequences; as these break down at different rates, this means that comparisons should be made between monogeneric samples. Sampling position is important in biominerals with complex microstructures [e.g., the different layers of calcite and aragonite found in *Patella* (87)], so this should be consistent and reported. Simple experimental tests determine whether biominerals are suitable for AA dating (e.g., ref. 88). Aminozone resolution will depend on the natural variability determined from age-equivalent samples for each taxa (89).

3.3.2. Impact of temperature. As a series of chemical reactions, protein breakdown in the IcP fraction will still be affected by temperature; without calibration, this temperature dependence limits AA dating to correlation between sites with similar integrated temperature histories. However, these regions can be quite large, covering several hundreds of kilometers (e.g., refs. 90 and 91). This necessarily impacts the age range possible using this technique, with samples from tropical regions having much shorter time ranges than temperate regions and polar regions having the longest resolvable time range.

The significant temperature differences between interglacial and glacial phases in the Pleistocene also need consideration, resulting in a nonlinear function with time (e.g., Fig. 5, which is reproduced from ref. 92). This also results in the temporal resolution differing significantly between interglacials (e.g., ±5 ka) and glacials (e.g., ±40 ka). Hence, evaluation of the stratigraphical context and any environmental indicators becomes important to the temporal interpretation of the AA data.

3.4. Application to Archaeological Questions and Development Potential. AA geochronology can provide a relative chronology and enable age correlation between sites, but it also allows numerical dates (e.g., Ar-Ar, U series), which are often only available from a very limited number of sites, to be extended to large numbers of sites where numerical age control is impossible. Currently, at archaeological sites, AA geochronology is most commonly conducted on mollusk shells and opercula, eggshell, and more recently, tooth enamel. To date, AA analysis of corals, foraminifera,

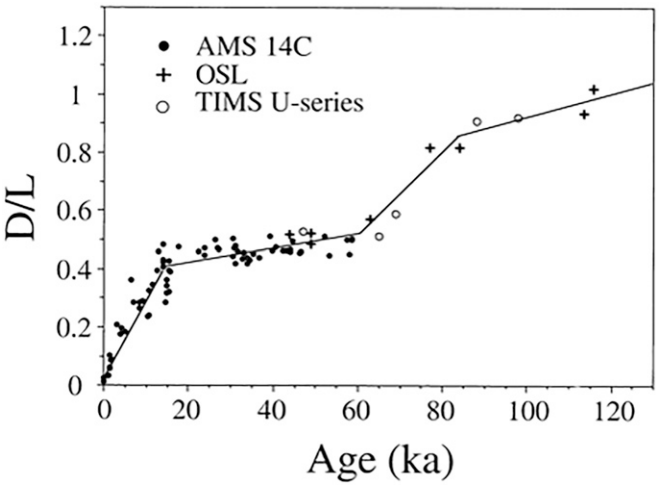

Fig. 5. Relationship between D/L values (in this case, D-alloisolucine/L-isoleucine; A/I) and years based on radiocarbon dates (measured by accelerator mass spectrometry; AMS), uranium-series (measured by thermal ionization mass spectrometry; TIMS), and luminescence dates. Note the stepwise nature of the increase in protein degradation with time due to relatively rapid racemization in warm phases and slowing of the reactions during cooler phases. Reproduced with permission from ref. 92 (AAAS).

and ostracods has mostly been undertaken to reconstruct paleoclimate, but as these biominerals are also found in archaeological sites, they could also form a dating substrate in these cases.

In most regions, the relatively slow rates of the AA reactions mean that the technique is most useful for dating Pleistocene samples. However, as it is a relatively inexpensive method, several studies of Holocene and Last Glacial archaeological material have exploited this by dating a small number of samples by ^{14}C but extending the dating study through the AA analysis of a larger number of samples (e.g., refs. 88, 93, and 94). Time averaging of deposits, which can be particularly prevalent in beach sediments (on the order of thousands of years) and archaeological middens (e.g., refs. 93 and 95), is also a critical factor to account for. This can be mitigated by analyzing higher numbers of samples per deposit and accounting for time averaging in the interpretation of the AA results.

Ratite eggshell AAs have provided important archaeological insights in Africa and Australia, pertinent to the debates on the timings and impact of the arrival of humans on faunal extinctions in Australia (92). In Africa, ostrich eggshell is commonly found in archaeological deposits from the last 200 ka, but the widespread use of hearths at these sites can impact the AA signal. Through key changes in IcP degradation behavior, heated eggshell can be identified and therefore, excluded from the dating evidence (e.g., refs. 96–98). Ostrich eggshell from the hominin site at Laetoli [3.8 Ma (99)] has also provided the currently oldest authenticated identification of an original protein sequence (and therefore, phylogenetic information).

In Bithyniid snails, the operculum (the structure that closes the aperture when the snail withdraws into its shell) is mineralized in the more stable form of calcium carbonate [calcite (100)] and preserves the IcP well in the fossil record. AA geochronology of *Bithynia* opercula has allowed correlation of Quaternary deposits with the MIS record (101–103), enabling archaeological sites to be correlated with specific interglacials and in some cases, to individual parts of the interglacial. This has provided an independent test of the temporal patterns in hominin occupations (Fig. 6) and in Paleolithic tool technology and development (102, 104).

Mammalian teeth are often a key component in archaeological deposits and so, are an excellent target for dating. Tooth enamel is highly mineralized, which bodes well for IcP preservation but proved particularly challenging for AA analyses; the high concentrations of inorganic salts in this calcium phosphate biomineral limited accurate quantification (105). Development of a new biphasic preparation method, tested first on elephantid tooth enamel (79, 106), shows that the rates of the reactions are significantly slower than those of calcium carbonate biominerals, which extends the time range of the enamel intracrystalline protein degradation (IcPD) method in temperate latitudes into the Pliocene. This technique has also been useful for testing the integrity of fossil protein in paleoproteomic studies,

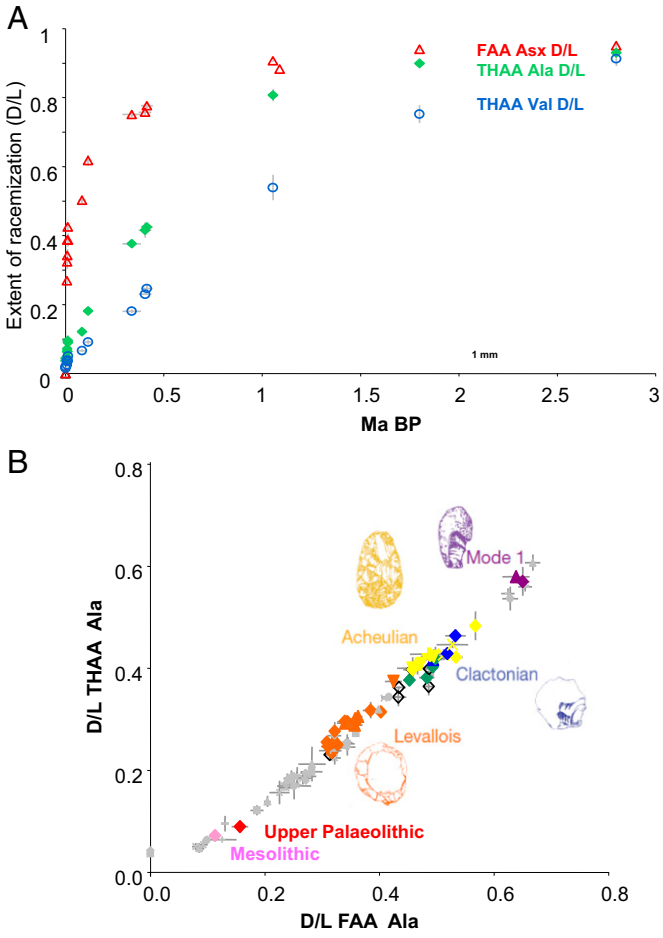

Fig. 6. (*A*) The increase in racemization in *Bithynia* opercula with age for the free amino acid (FAA) aspartic acid (Asx) and the total hydrolysable amino acids (THAAs) valine (Val) and alanine (Ala). Asx racemizes rapidly and is, therefore, most valuable for separating sites younger than ~200 ka. Val racemizes more slowly and is able to differentiate between sites back to the Pliocene, but it provides poorer resolution for young sites. Using multiple AAs with different rates of degradation, therefore, enables greater time depth and age resolution. (*B*) Mean THAA D/L vs. FAA D/L for alanine in *Bithynia* opercula from British sites; these two measures of breakdown should be highly correlated in a closed system, and so, this plot forms an aminostratigraphic framework, where young samples fall toward the bottom left and old samples lie toward the top right of the graph. These frameworks allow for temporal exploration of the archaeological record, with sites color coded by occurrence of technology (green signifies both Clactonian and Acheulian at a site). Modified from ref. 102.

confirming the endogeneity of 1.78 Ma protein from rhino enamel from the Paleolithic site of Dmanisi (107) and demonstrating the enormous potential for the preserved protein in mammalian tooth enamel to provide evolutionary relationships on directly dated samples. As preparation procedures are refined, resulting in reduced sample sizes, the prospect of analysis of closed system protein from hominin tooth enamel is now being realized (108).

4. Conclusions

Over the last few decades, an appreciation of the complexities, limitations, and strengths of trapped charge and AA geochronologies has resulted in a range of developments. These two approaches have transformed our view of the Paleolithic by providing a chronology beyond the limit of radiocarbon dating, and the methods can be applied in almost any part of the world.

In luminescence and ESR, the discovery of an increasingly diverse range of signals has made it possible to calculate multiple ages for a sample (e.g., with quartz OSL and TT-OSL or with Ti and Al centers in ESR), providing the opportunity to corroborate results. Different signals also cover different time ranges, allowing both ESR and luminescence to address a wide range of archaeological materials over different time periods. The introduction of new optical stimulation sources and detectors has also extended the range of signals and sample materials that can be analyzed. Most focus has been on the development of increasingly sophisticated methods of D_e determination, and similar emphasis needs to be placed on the dose rate in future research. In ESR, the development of coupled U-series and ESR measurements on teeth exploited developments in laser ablation ICP-MS. Similarly, detailed analysis of the dose rate for ESR of sediments and luminescence dating would help to provide even greater confidence in the ages determined using trapped charge dating.

In AA geochronology, analysis of multiple D/L pairs (through new chromatography methods) and identification of fossil IcP have provided greater accuracy in AA dating results. Analysis of different biominerals extends the dating frameworks across a wide range of environments and archaeological research questions. Thanks to agreement by the AA community to archive published fossil data, the added value of sharing these datasets for regional and global comparisons is being realized, with open access at https://www.ncdc.noaa.gov/paleo/aar.html.

Trapped charge and AA geochronologies both measure the time signals trapped within the crystals of sediment and/or fossils; by exploiting this across a range of archaeological sites, these two complementary dating approaches have great potential for unlocking the Paleolithic.

Data Availability. As this is a review paper, all study data are included in the referenced papers.

ACKNOWLEDGMENTS. We thank our Quaternary colleagues over the years for their valuable advice and discussions, and Lucy Wheeler for preparing part of Fig. 4*A*. This paper arose from a project that received funding from the European Research Council under the European Union's Horizon 2020 Research and Innovation Programme Grant 865222 ("EQuaTe–Bridging Europe: A Quaternary Timescale for the Expansion and Evolution of Humans").

1. J. J. Lowe, M. J. C. Walker, *Reconstructing Quaternary Environments* (Routledge, ed. 3, 2015).
2. M. Walker, *Quaternary Dating Methods* (John Wiley & Sons, Chichester, United Kingdom, 2005).
3. M. J. Aitken, *Thermoluminescence Dating* (Academic Press, London, United Kingdom, 1985).
4. M. Duval, "Dating and electron spin resonance (ESR)" in *The Encyclopedia of Archaeological Sciences*, S. L. López Varela, Ed. (Wiley-Blackwell, 2018), https://doi.org/10.1002/9781119188230.saseas0148.
5. M. Duval, L. J. Arnold, G. Rixhon, Electron spin resonance dating in quaternary studies: Evolution, recent advances and applications. *Quat. Int.* **556**, 1–10 (2020).
6. G. A. T. Duller, *Luminescence Dating: Guidelines on Using Luminescence Dating in Archaeology* (English Heritage Publishing, 2008).
7. A. G. Wintle, Fifty years of luminescence dating. *Archaeometry* **50**, 276–312 (2008).
8. R. G. Roberts *et al.*, Optical dating in archaeology: Thirty years in retrospect and grand challenges for the future. *J. Archaeol. Sci.* **56**, 41–60 (2015).
9. M. Ikeya, Dating a stalactite by electron paramagnetic resonance. *Nature* **255**, 48–50 (1975).
10. M. Ikeya, *New Applications of Electron Spin Resonance Dating, Dosimetry and Microscopy* (World Scientific, Singapore, 1993).
11. R. Grün *et al.*, Direct dating of Florisbad hominid. *Nature* **382**, 500–501 (1996).
12. R. Grün, H. P. Schwarcz, J. Chadam, Electron spin-resonance dating of tooth enamel-coupled correction for U-uptake and U-series disequilibrium. *Nucl. Tracks Radiat. Meas.* **14**, 237–241 (1988).
13. R. Grün, S. Eggins, L. Kinsley, H. Moseley, M. Sambridge, Laser ablation U-series analysis of fossil bones and teeth. *Palaeogeogr. Palaeoclimatol. Palaeoecol.* **416**, 150–167 (2014).
14. P. H. G. M. Dirks *et al.*, The age of *Homo naledi* and associated sediments in the Rising Star Cave, South Africa. *eLife* **6**, e24231 (2017).
15. M. Duval *et al.*, The first direct ESR dating of a hominin tooth from Atapuerca Gran Dolina TD-6 (Spain) supports the antiquity of Homo antecessor. *Quat. Geochronol.* **47**, 120–137 (2018).
16. R. Grün, A very personal, 35 years long journey in ESR dating. *Quat. Int.* **556**, 20–37 (2020).
17. Y. Yokoyama, C. Falgueres, J. P. Quaegebeur, ESR dating of quartz from Quaternary sediments: First attempt. *Nucl. Tracks Radiat. Meas.* **10**, 921–928 (1985).
18. S. Toyoda, Paramagnetic lattice defects in quartz for applications to ESR dating. *Quat. Geochronol.* **30**, 498–505 (2015).
19. H. Tissoux *et al.*, Potential use of Ti-center in ESR dating of fluvial sediment. *Quat. Geochronol.* **2**, 367–372 (2007).
20. P. Voinchet *et al.*, Artificial optical bleaching of the Aluminium center in quartz implications to ESR dating of sediments. *Quat. Sci. Rev.* **22**, 1335–1338 (2003).
21. S. Tsukamoto *et al.*, Quartz natural and laboratory ESR dose response curves: A first attempt from Chinese loess. *Radiat. Meas.* **120**, 137–142 (2018).
22. P. Voinchet *et al.*, New chronological data (ESR and ESR/U-series) for the earliest Acheulian sites of north-western Europe. *J. Quaternary Sci.* **30**, 610–622 (2015).
23. P. Antoine *et al.*, The earliest evidence of Acheulian occupation in Northwest Europe and the rediscovery of the Moulin Quignon site, Somme valley, France. *Sci. Rep.* **9**, 13091 (2019).
24. J. J. Bahain *et al.*, ESR and ESR/U-series chronology of the Middle Pleistocene site of Tourvillela-Riviere (Normandy, France): A multi-laboratory approach. *Quat. Int.* **556**, 66–78 (2020).
25. S. Toyoda, P. Voinchet, C. Falguères, J. M. Dolo, M. Laurent, Bleaching of ESR signals by the sunlight: A laboratory experiment for establishing the ESR dating of sediments. *Appl. Radiat. Isot.* **52**, 1357–1362 (2000).
26. D. J. Huntley, D. I. Godfrey-Smith, M. L. W. Thewalt, Optical dating of sediments. *Nature* **313**, 105–107 (1985).
27. N. A. Spooner, D. G. Questiaux, Kinetics of red, blue and UV thermoluminescence and optically-stimulated luminescence from quartz. *Radiat. Meas.* **32**, 659–666 (2000).
28. G. A. T. Duller, Single grain optical dating of Quaternary sediments: Why aliquot size matters in luminescence dating. *Boreas* **37**, 589–612 (2008).
29. C. Clarkson *et al.*, Human occupation of northern Australia by 65,000 years ago. *Nature* **547**, 306–310 (2017).
30. Z. Jacobs, A. G. Wintle, G. A. T. Duller, R. G. Roberts, L. Wadley, New ages for the post-Howiesons Poort, late and final Middle Stone Age at Sibudu, South Africa. *J. Archaeol. Sci.* **35**, 1790–1807 (2008).
31. R. F. Galbraith, R. G. Roberts, Statistical aspects of equivalent dose and error calculation and display in OSL dating: An overview and some recommendations. *Quat. Geochronol.* **11**, 1–27 (2012).
32. Y. S. Mayya, P. Morthekai, M. K. Murari, A. K. Singhvi, Towards quantifying beta microdosimetric effects in single-grain quartz dose distribution. *Radiat. Meas.* **41**, 1032–1039 (2006).
33. F. Fang *et al.*, 2D modelling: A Monte Carlo approach for assessing heterogeneous beta dose rates in luminescence and ESR dating. Paper II, application to igneous rocks. *Quat. Geochronol.* **48**, 195–206 (2018).
34. R. K. Smedley, G. A. T. Duller, D. Rufer, J. E. P. Utley, Empirical assessment of beta dose heterogeneity in sediments: Implications for luminescence dating. *Quat. Geochronol.* **56**, 101052 (2020).
35. G. A. T. Duller, Improving the accuracy and precision of equivalent doses determined using the optically stimulated luminescence signal from single grains of quartz. *Radiat. Meas.* **47**, 770–777 (2012).
36. K. J. Thomsen *et al.*, Testing single-grain quartz OSL methods using sediment samples with independent age control from the Bordes-Fitte rockshelter (Roches d'Abilly site, Central France). *Quat. Geochronol.* **31**, 77–96 (2016).
37. M. S. Chapot, H. M. Roberts, G. A. T. Duller, Z. P. Lai, A comparison of natural- and laboratory-generated dose response curves for quartz optically stimulated luminescence signals from Chinese loess. *Radiat. Meas.* **47**, 1045–1052 (2012).
38. X. L. Wang, Y. C. Lu, A. G. Wintle, Recuperated OSL dating of fine-grained quartz in Chinese loess. *Quat. Geochronol.* **1**, 89–100 (2006).

39. L. J. Arnold *et al.*, Evaluating the suitability of extended-range luminescence dating techniques over early and Middle Pleistocene timescales: Published datasets and case studies from Atapuerca, Spain. *Quat. Int.* **389**, 167–190 (2015).
40. J. L. Arsuaga *et al.*, Neandertal roots: Cranial and chronological evidence from Sima de los Huesos. *Science* **344**, 1358–1363 (2014).
41. G. A. T. Duller, S. Tooth, L. Barham, S. Tsukamoto, New archaeological investigations at Kalambo Falls, Zambia: Luminescence chronology and site formation. *J. Hum. Evol.* **85**, 111–125 (2015).
42. M. Chazan *et al.*, Archeology, environment, and chronology of the Early Middle Stone Age component of Wonderwerk Cave. *J. Paleolithic Arch.* **3**, 302–335 (2020).
43. G. Adamiec, G. A. T. Duller, H. M. Roberts, A. G. Wintle, Improving the TT-OSL SAR protocol through source trap characterisation. *Radiat. Meas.* **45**, 768–777 (2010).
44. G. Faershtein, B. Guralnik, R. Lambert, A. Matmon, N. Porat, Investigating the thermal stability of TT-OSL main source trap. *Radiat. Meas.* **119**, 102–111 (2018).
45. L. J. Arnold, M. Demuro, Insights into TT-OSL signal stability from single-grain analyses of known-age deposits at Atapuerca, Spain. *Quat. Geochronol.* **30**, 472–478 (2015).
46. I. K. Bailiff, D. Bridgland, P. P. Cunha, Extending the range of optically stimulated luminescence dating using vein-quartz and quartzite sedimentary pebbles. *Quat. Geochronol.* **65**, 101180 (2021).
47. A. G. Wintle, Anomalous fading of thermoluminescence in mineral samples. *Nature* **245**, 143–144 (1973).
48. D. J. Huntley, M. Lamothe, Ubiquity of anomalous fading in K-feldspars and the measurement and correction for it in optical dating. *Can. J. Earth Sci.* **38**, 1093–1106 (2001).
49. K. J. Thomsen, A. S. Murray, M. Jain, L. Bøtter-Jensen, Laboratory fading rates of various luminescence signals from feldspar-rich sediment extracts. *Radiat. Meas.* **43**, 1474–1486 (2008).
50. D. Colarossi, G. A. T. Duller, H. M. Roberts, Exploring the behaviour of luminescence signals from feldspars: Implications for the single aliquot regenerative dose protocol. *Radiat. Meas.* **109**, 35–44 (2018).
51. H. M. Roberts, C. L. Bryant, D. G. Huws, H. F. Lamb, Generating long chronologies for lacustrine sediments using luminescence dating: A 250,000 year record from Lake Tana, Ethiopia. *Quat. Sci. Rev.* **202**, 66–77 (2018).
52. Z. Jacobs *et al.*, Timing of archaic hominin occupation of Denisova Cave in southern Siberia. *Nature* **565**, 594–599 (2019).
53. E. I. Zavala *et al.*, Pleistocene sediment DNA reveals hominin and faunal turnovers at Denisova Cave. *Nature* **595**, 399–403 (2021).
54. D. Richter, Advantages and limitations of thermoluminescence dating of heated flint from paleolithic sites. *Geoarchaeology* **22**, 671–683 (2007).
55. D. Richter *et al.*, The age of the hominin fossils from Jebel Irhoud, Morocco, and the origins of the Middle Stone Age. *Nature* **546**, 293–296 (2017).
56. F. Daniels, C. A. Boyd, D. F. Saunders, Thermoluminescence as a research tool. *Science* **117**, 343–349 (1953).
57. N. M. Johnson, Thermoluminescence in biogenic calcium carbonate. *J. Sediment. Petrol.* **30**, 305–313 (1960).
58. G. A. T. Duller, K. E. H. Penkman, A. G. Wintle, Assessing the potential for using biogenic calcites as dosimeters for luminescence dating. *Radiat. Meas.* **44**, 429–433 (2009).
59. R. J. Stirling, G. A. T. Duller, H. M. Roberts, Developing a single-aliquot protocol for measuring equivalent dose in biogenic carbonates. *Radiat. Meas.* **47**, 725–731 (2012).
60. G. A. T. Duller, M. Kook, R. J. Stirling, H. M. Roberts, A. S. Murray, Spatially-resolved thermoluminescence from snail opercula using an EMCCD. *Radiat. Meas.* **81**, 157–162 (2015).
61. G. A. T. Duller, H. M. Roberts, Seeing snails in a new light: Luminescence dating using calcite. *Elements* **14**, 39–43 (2018).
62. D. R. Bridgland *et al.*, An enhanced record of MIS 9 environments, geochronology and geoarchaeology: Data from construction of the High Speed 1 (London-Channel Tunnel) rail-link and other recent investigations at Purfleet, Essex, UK. *Proc. Geol. Assoc.* **124**, 417–476 (2013).
63. K. Penkman, "Amino acid racemization dating" in *Encyclopedia of Geology*, D. Alderton, S. A., Elias, Eds. (Elsevier, ed. 2, 2021), pp. 175–186.
64. J. L. Bada, "Non-equilibrium systems in natural water chemistry" in *Advances in Chemistry*, J. D. Hem, R. F. Gould, Eds. (American Chemical Society, Washington, DC, 1971), vol. **106**, pp. 309–331.
65. J. Wehmiller, P. E. Hare, Racemization of amino acids in marine sediments. *Science* **173**, 907–911 (1971).
66. N. Kriausakul, R. M. Mitterer, Isoleucine epimerization in peptides and proteins: Kinetic factors and application to fossil proteins. *Science* **201**, 1011–1014 (1978).
67. G. G. Smith, R. C. Evans, "The effect of structure and conditions on the rate of racemisation of free and bound amino acids" in *Biogeochemistry of Amino Acids*, P. E. Hare, T. C. Hoering, K. King Jr., Eds. (Wiley, New York, NY, 1980), pp. 257–282.
68. B. Demarchi *et al.*, New experimental evidence for in-chain amino acid racemization of serine in a model peptide. *Anal. Chem.* **85**, 5835–5842 (2013).
69. P. E. Hare, "Organic geochemistry of bones, and its relation to the survival of bone in the natural environment" in *Fossils in the Making*, A. K. Behrensmeyer, A. P. Hill, Eds. (Chicago University, Chicago, IL, 1980), pp. 208–219.
70. G. H. Miller, D. M. Hopkins, "Degradation of molluscan shell protein by lava-induces transient heat flow, Pribilof Islands, Alaska: Implications for amino acid geochronology and radiocarbon dating" in *Biogeochemistry of Amino Acids*, P. E. Hare, T. C. Hoering, K. King Jr., Eds. (Wiley, New York, NY, 1980), pp. 445–451.
71. T. C. Hoering, "The organic constituent of fossil mollusc shells" in *Biogeochemistry of Amino Acids*, P. E. Hare, T. C. Hoering, K. King Jr., Eds. (Wiley, New York, NY, 1980), pp. 193–201.
72. K. M. Towe, "Preserved organic ultrastructure: An unreliable indicator for Paleozoic amino acid biogeochemistry" in *Biogeochemistry of Amino Acids*, P. E. Hare, T. C. Hoering, K. King Jr., Eds. (Wiley, New York, NY, 1980), pp. 65–74.
73. A. S. Brooks *et al.*, Dating pleistocene archeological sites by protein diagenesis in ostrich eggshell. *Science* **248**, 60–64 (1990).
74. G. H. Miller, C. P. Hart, E. B. Roark, B. J. Johnson, "Isoleucine epimerization in eggshells of the flightless Australian birds *Genyornis* and *Dromaius*" in *Perspectives in Amino Acid and Protein Geochemistry*, G. A. Goodfriend, M. J. Collins, M. L. Fogel, S. A. Macko, J. F. Wehmiller, Eds. (Oxford University Press, Oxford, United Kingdom, 2000), pp. 161–181.
75. K. Gries, R. Kröger, C. Kübel, M. Fritz, A. Rosenauer, Investigations of voids in the aragonite platelets of nacre. *Acta Biomater.* **5**, 3038–3044 (2009).
76. M. A. Crenshaw, The soluble matrix from *Mercenaria* shell. *Biomineralisation* **6**, 6–11 (1972).
77. G. A. Sykes, M. J. Collins, D. I. Walton, The significance of a geochemically isolated intracrystalline fraction within biominerals. *Org. Geochem.* **23**, 1059–1065 (1995).
78. K. E. H. Penkman, D. S. Kaufman, D. Maddy, M. J. Collins, Closed-system behaviour of the intra-crystalline fraction of amino acids in mollusc shells. *Quat. Geochronol.* **3**, 2–25 (2008).
79. M. Dickinson, A. M. Lister, K. E. H. Penkman, A new method for enamel amino acid racemization dating: A closed system approach. *Quat. Geochronol.* **50**, 29–46 (2019).
80. C. A. Orem, D. S. Kaufman, Effects of basic pH on amino acid racemization and leaching in mollusc shell. *Quat. Geochronol.* **6**, 233–245 (2011).
81. J. Bright, D. S. Kaufman, Amino acid racemization in lacustrine ostracodes, part I: Effect of oxidising pre-treatments on amino acid composition. *Quat. Geochronol.* **6**, 154–173 (2011).
82. B. Demarchi *et al.*, Testing the effect of bleaching on the bivalve *Glycymeris*: A case study of amino acid geochronology on key Mediterranean raised beach deposits. *Quat. Geochronol.* **25**, 49–65 (2015).
83. J. E. Ortiz, T. Torres, Y. Sánchez-Palencia, M. Ferrer, Inter- and intra-crystalline protein diagenesis in *Glycymeris* shells: Implications for amino acid geochronology. *Quat. Geochronol.* **41**, 37–50 (2017).
84. E. J. Hendy *et al.*, Assessing amino acid racemization variability in coral intra-crystalline protein for geochronological applications. *Geochim. Cosmochim. Acta* **86**, 338–353 (2012).
85. A. R. Nelson, *Quaternary Glacial and Marine Stratigraphy of the Qivitu Peninsula, Northern Cumberland Peninsula, Baffin Island, Canada* (University of Colorado, Boulder, CO, 1978).
86. G. H. Miller, P. E. Hare, "Amino acid geochronology: Integrity of the carbonate matrix and potential of molluscan fossils" in *Biogeochemistry of Amino Acids*, P. E. Hare, T. C. Hoering, K. King Jr., Eds. (Wiley, New York, NY, 1980), pp. 415–443.
87. J. E. Ortiz, I. Gutiérrez-Zugasti, T. Torres, M. González-Morales, Y. Sánchez-Palencia, Protein diagenesis in *Patella* shells: Implication for amino acid racemisation dating. *Quat. Geochronol.* **27**, 105–118 (2015).
88. B. Demarchi *et al.*, AAR dating of shell middens: A mound of possibilities. *Quat. Int.* **239**, 114–124 (2011).
89. J. F. Wehmiller, G. H. Miller, "Aminostratigraphic dating methods in Quaternary geology" in *Quaternary Geochronology: Methods and Applications*, J. Stratton Noller, J. M. Sowers, W. R. Lettis, Eds. (American Geophysical Union, Washington, DC, 2000), pp. 187–222.
90. J. F. Wehmiller, United States Quaternary coastal sequences and molluscan racemization geochronology: What have they meant for each other over the past 45 years? *Quat. Geochronol.* **16**, 3–20 (2013).
91. M. J. Sier *et al.*, Direct terrestrial-marine correlation demonstrates surprisingly late onset of the last interglacial in central Europe. *Quat. Res.* **75**, 213–218 (2011).
92. G. H. Miller *et al.*, Pleistocene extinction of *Genyornis newtoni*: Human impact on Australian megafauna. *Science* **283**, 205–208 (1999).
93. B. Koppel, K. Szabo, M. W. Moore, M. J. Morwood, Untangling time-averaging in shell middens: Defining temporal units using amino acid racemisation. *J. Archaeol. Sci. Rep.* **7**, 741–750 (2016).
94. J. E. Ortiz, Y. Sánchez-Palencia, I. Gutiérrez-Zugasti, T. Torres, M. González-Morales, Protein diagenesis in archaeological gastropod shells and the suitability of this material for amino acid racemisation dating: *Phorcus lineatus* (da Costa, 1778). *Quat. Geochronol.* **46**, 16–27 (2018).
95. M. Kowalewski, G. A. Goodfriend, K. W. Flessa, High resolution estimates of temporal mixing within shell beds: The evils and virtues of time-averaging. *Palaeobiol.* **24**, 287–304 (1998).
96. A. S. Brooks, P. E. Hare, J. E. Kokis, K. Durana, A burning question: Differences between laboratory-induced and natural diagenesis in ostrich eggshell proteins. *Carnegie Inst. Washington Yearbook* **2250**, 176–179 (1991).
97. G. H. Miller, P. B. Beaumont, A. J. Jull, B. Johnson, Pleistocene geochronology and palaeothermometry from protein diagenesis in ostrich eggshells: Implications for the evolution of modern humans. *Philos. Trans. R. Soc. Lond. B Biol. Sci.* **337**, 149–157 (1992).
98. C. V. Murray-Wallace, J. Richter, R. Vogelsang, Aminostratigraphy and taphonomy of ostrich eggshell in the sedimentary infill of Apollo 11 Rockshelter, Namibia. *J. Archaeol. Sci. Rep.* **4**, 143–151 (2015).
99. B. Demarchi *et al.*, Protein sequences bound to mineral surfaces persist into deep time. *eLife* **5**, e17092 (2016).
100. K. E. H. Penkman, R. C. Preece, D. H. Keen, M. J. Collins, Amino acid geochronology of the type Cromerian of West Runton, Norfolk, UK. *Quat. Int.* **228**, 25–37 (2010).
101. K. E. H. Penkman *et al.*, An aminostratigraphy for the British Quaternary based on *Bithynia* opercula. *Quat. Sci. Rev.* **61**, 111–134 (2013).
102. K. E. H. Penkman *et al.*, A chronological framework for the British Quaternary based on *Bithynia* opercula. *Nature* **476**, 446–449 (2011).
103. A. S. Tesakov *et al.*, Aminostratigraphical test of the East European Mammal Zonation for the late Neogene and Quaternary. *Quat. Sci. Rev.* **245**, 106434 (2020).
104. M. J. White, D. R. Bridgland, D. C. Schreve, T. E. White, K. E. H. Penkman, Well-dated fluvial sequences as templates for patterns of handaxe distribution: Understanding the record of Acheulian activity in the Thames and its correlatives. *Quat. Int.* **480**, 118–131 (2018).
105. R. Griffin, *Application of Amino Acid Racemization in Enamel to the Age Estimation of Age at Death of Archaeological Remains* (University of York, York, United Kingdom, 2006).
106. S. Baleka *et al.*, Estimating the dwarfing rate of an extinct Sicilian elephant. *Curr. Biol.* **31**, 3606–3612.e7 (2021).
107. E. Cappellini *et al.*, Early Pleistocene enamel proteome from Dmanisi resolves Stephanorhinus phylogeny. *Nature* **574**, 103–107 (2019).
108. F. Welker *et al.*, The dental proteome of Homo antecessor. *Nature* **580**, 235–238 (2020).